Wiley
Journal of Food Biochemistry
Volume 2024, Article ID 5521656, 12 pages
https://doi.org/10.1155/2024/5521656

WILEY

Research Article

Characterization of *Anoectochilus roxburghii* Bioactive Compounds and Its Inhibition on the Metabolism-Related Enzyme Activities *In Vitro*

Jiahao Yuan,[1] Xiuna Wu,[1] Emad Karrar,[1] Lingyu Zhang,[1,2] Zhiyong Huang,[1,2] Daren Wu ,[1,2] and Jian Li [1,2]

[1]*College of Food and Biological Engineering, Jimei University, Xiamen 361021, China*
[2]*Fujian Provincial Engineering Technology Research Center of Marine Functional Food, Xiamen 361021, China*

Correspondence should be addressed to Daren Wu; darrenwu@jmu.edu.cn and Jian Li; lijian2013@jmu.edu.cn

Received 16 April 2024; Revised 4 June 2024; Accepted 20 June 2024

Academic Editor: Xiaoyu Song

Copyright © 2024 Jiahao Yuan et al. This is an open access article distributed under the Creative Commons Attribution License, which permits unrestricted use, distribution, and reproduction in any medium, provided the original work is properly cited.

In this study, the *Anoectochilus roxburghii* (*A. roxburghii*) was studied for its chemical composition and biological activities. The first aim of this work was to isolate and purify compounds from *A. roxburghii* using Sephadex LH-20 and HPLC. The identification of seven compounds was achieved, with 5,4′-dihydroxy-3,3′,7-trimethoxy-flavone and 5-hydroxy-3,4-dimethyl-5-pentylfuran-2(5H)-one being isolated from *A. roxburghii* for the first time. The second aim was to describe its inhibition on the metabolism-related enzyme activities *in vitro*. Further, 3,5-dihydroxy-7,3′,4′-trimethoxyflavone and 5-hydroxy-3,4-dimethyl-5-pentylfuran-2(5H)-one showed inhibitory activity on xanthine oxidase, while isorhamnetin-3-O-rutinoside ($IC_{50} = 87.45\,\mu g/mL$) may be potential inhibitors of α-amylase. Molecular docking analysis revealed that isorhamnetin-3-O-rutinoside exhibited the highest binding affinity towards PL. In addition to scientifically expanding the compound library of *A. roxburghii*, the discovery is also a vital reference for finding new insights in the field of medication research, especially as natural metabolism-related enzyme inhibitors.

1. Introduction

Anoectochilus roxburghii (Wall.) Lindl. is a perennial herb belonging to the genus *Anoectochilus* of the Orchidaceae family [1]. The plant has a mild and sweet flavor, making it widely utilized as a medicinal and food homologous agent among the populace [2]. It contains polysaccharides, steroidal compounds, organic acids, terpenoids, alkaloids, volatile oils, flavonoids, and glycosides [3]. Furthermore, it also has anti-inflammatory [4], anti-rheumatoid arthritis [5], hepatoprotective [6], antioxidant properties [3], andanti-hyperglycemic [7] effects. Although *A. roxburghii* has such pharmacological activities, on the one hand, the specific ingredients that affect these pharmacological activities are not clear enough; on the other hand, there are no in-depth reports on its uric acid-lowering, hypoglycemic, and hypolipidemic properties, and it needs to be explored. Diabetes is a significant metabolic disorder characterized by insulin resistance, aberrant glucose metabolism, heightened oxidative stress, and the onset of pathogenic conditions such as neuropathy, retinopathy, and obesity [8]. In humans, α-amylase (αA) is an enzyme responsible for the hydrolysis of starch [9]. Diabetes complications can be effectively managed through inhibition of αA, which delays or suppresses glucose absorption into the small intestine.

Hyperuricemia (HUA), characterized by dysregulation in purine metabolism, exhibits a high prevalence among Chinese adults, ranging from 8.4 to 13.3% [10]. Emerging evidence suggests that HUA can give rise to diverse manifestations of multiorgan dysfunction, encompassing renal impairment, hepatic abnormalities, disruptions in endocrine and metabolic homeostasis, and cerebrovascular and cardiovascular disorders [11]. Xanthine oxidase (XOD) serves as the pivotal enzyme accountable for catalyzing

hypoxanthine into xanthine and subsequently converting xanthine into uric acid, thereby playing a crucial role in developing HUA and gout. Currently, allopurinol and febuxostat have obtained clinical approval as XOD inhibitors for managing HUA and gout disease. However, due to adverse effects associated with these XOD inhibitors, such as hepatitis, nephropathy, and allergic reaction [12], there is an urgent need to explore novel natural alternatives that ensure safer consumption. Bioactive substances of plant origin may be a good choice.

Hyperlipidemia is characterized as a disorder involving disturbances in lipid metabolism, including elevated levels of total cholesterol (TC), triglyceride (TG), and low-density lipoprotein cholesterol (LDL-C), along with reduced levels of high-density lipoprotein cholesterol [13]. Dysregulated lipid profiles significantly contribute to the risk of cardiovascular disease, posing a grave threat to human health. Pancreatic lipase (PL) is pivotal in triglyceride absorption within lipid metabolism [14]. Inhibiting lipase activity is considered an effective mechanism for impeding triacylglyceride absorption in patients with hypercholesterolemia.

There is a wealth of natural biological resources and traditional medicinal knowledge in China, encompassing diverse folk and ethnic medicines. However, there are still numerous species that remain understudied and underutilized, with some lacking chemical investigation. Consequently, the pursuit of novel drugs derived from natural sources that exhibit high efficacy, low toxicity, and targeted specificity for treating metabolic diseases has emerged as a pivotal focus within drug research and development. The screening of plant extracts for pharmacological activity, followed by subsequent trials to identify their bioactive ingredients, has led to the discovery of numerous pharmacologically valuable substances exhibiting potential hypoglycemic, uric acid-lowering, and hypolipidemic properties. Since *A. roxburghii* contains various bioactive ingredients and shows good pharmacological activity, our purpose was to investigate these bioactive compounds from the dried products of *A. roxburghii* and analyze their chemical structure, combining molecular simulation to find potential biologically active substances. To isolate these compounds from the dried products of *A. roxburghii*, 70% ethanol extraction, Sephadex LH-20, reversed-phase C18 (RP-C18), thin-layer chromatography (TLC), and high-performance liquid chromatography (HPLC) were employed. Nuclear magnetic resonance spectroscopy (NMR) determined the compound's structure. The impact of these compounds on the enzyme activity of αA, XOD, and PL was further investigated. Additionally, a molecular docking analysis was conducted to study the structure-activity relationship. The experimental findings significantly contributed to the investigation the bioactive compounds in *A. roxburghii* and the activities of metabolism-related enzyme *in vitro*. A graphic abstract of our study is depicted in Figure 1.

2. Materials and Methods

2.1. Reagents and Chemicals. Various chemicals and reagents were obtained from different suppliers for experiments. The following reagents were purchased from Sinopharm Chemical Reagent Co. Ltd.: methanol (MeOH), AcOEt (ethyl acetate), ethanol (EtOH), isopropyl alcohol, sodium dihydrogen phosphate, dimethyl sulfoxide (DMSO), and sodium dihydrogen phosphate. HPLC quality methanol and acetonitrile were also acquired from the Merck Company in Germany. DNS (3,5-dinitrosalicylic acid) was procured from Beijing Soleibao Co. Ltd. XOD, αA, xanthine, allopurinol, and acarbose (50 mg/tablet) were provided by Tokyo Chemical Industries Co. Ltd. (Tokyo, Japan). Shanghai Macklin Biochemical Technology Co. Ltd. provided a final supply of PL, p-nitrophenyl palmitate, and orlistat.

2.2. Plant Material. The *A. roxburghii* specimen, which was one year old, was obtained from Zhangzhou Meilide Biological Engineering Co. Ltd. The specimen was dehydrated in an industrial oven at 85°C for hours. Afterwards, the meticulously ground desiccated samples underwent milling using a No. 2 sieve on a milling apparatus.

2.3. Extraction of Bioactive Compounds. The weighed dried powders, which amounted to 700 grams, underwent five cycles of extraction at 25°C for one hour using a ratio of 1000 mL of 70% ethanol per every 0.1 kg of dried raw material. Then, the organic solvent was removed through rotary evaporation, resulting in a crude extract weighing 324 g. Subsequently, the crude ethanol extract was resuspended with 1000 mL ice-cold ultra-pure water. The resulting extract was then partitioned with EtOAc (1000 mL) to afford the EtOAc portion (21.2 g). Furthermore, the EtOAc portion (21.2 g) was subjected to fractionation using medium-pressure reversed-phase C18 column (YMC-Pack ODS-AQ-HG). The column employed in this process is designed to withstand high pressure and provides optimal separation of the target compounds. Subsequently, TLC analysis was performed to confirm the components contained in each fraction. In addition, further refinement of the separation process was performed using the Sephadex LH-20 column. Then, the fractions were gathered and consolidated based on their similarities, resulting in major fractions. This step was essential in concentrating the target compounds and ensuring the highest purity levels. The purification of compounds and the assessment of their purity were then conducted using quantitative HPLC. Ultimately, seven compounds were successfully isolated from *A. roxburghii* after a series of intricate processes.

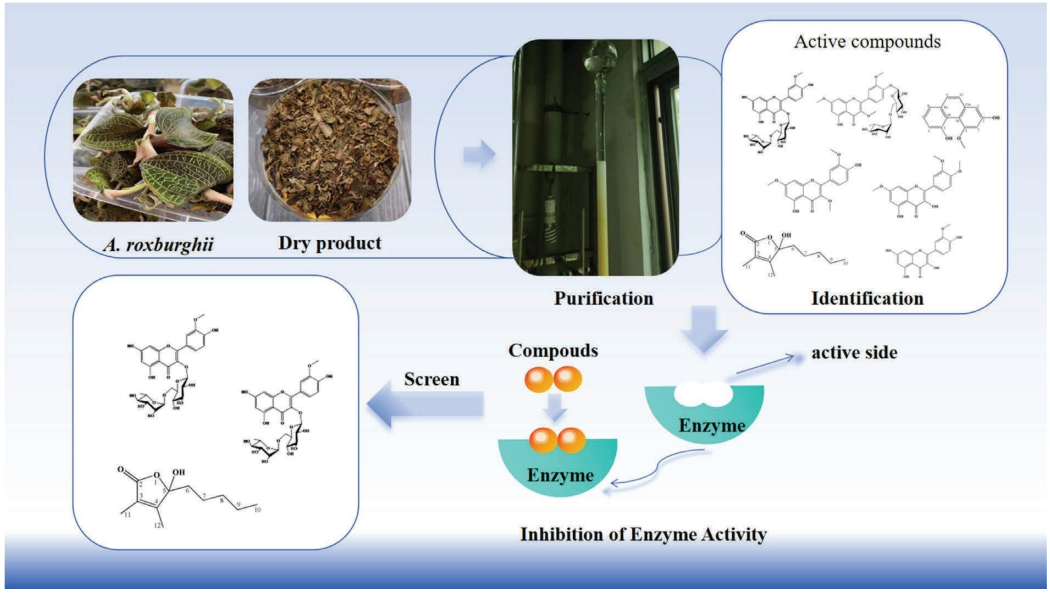


FIGURE 1: Graphic abstract. Figure depicts a graphic abstract of the present study.

2.4. HPLC Analysis. Analyses of compounds were carried out with an Agilent Technologies 1260 liquid chromatograph (Aglient Technologies, Waldbronn, Germany) equipped with a diode array detector (DAD). For the separation of components in the extracts of *A. roxburghii*, a high-performance Welch Ultimate LP-C_{18} column (with a particle size of 5 μm, 250 mm × 4.6 mm) was employed. The mobile phase used in the chromatographic process was a mixture of methanol (A) and 0.1% formic acid in water (B) (5 : 95, v/v). The flow rate was 1.0 mL/min, and the consistency was constant. Each stock solution was diluted with methanol to achieve a final 0.1 mg/mL concentration for analysis. This was followed by filtration through a filter with 0.45 μm pores to remove any potential impurities and ensure the purity of the sample. The column was conditioned at a temperature of 15°C, and the sample injection volume was set at 20 μL to ensure accurate and precise measurement of the target compounds.

2.5. NMR Spectroscopy. The ^{1}H NMR (500 MHz) and ^{13}C NMR (125 MHz) spectra were recorded using an AvanceII-500 spectrometer model manufactured by Bruker in Switzerland. The sample was dissolved in CD_3OD (0.6 mL) and maintained at a temperature of 300 K during analysis. Furthermore, all chemical shifts of both ^{1}H and ^{13}C were referenced to TMS (tetramethylsilane), a stable internal standard used in NMR spectroscopy to define the zero point of the chemical shift scale. This referencing process allowed for an accurate comparison of the sample's chemical shifts with those of known compounds, aiding in the identification and characterization of the sample.

2.6. Mass Spectrometry Conditions. The analyzed samples were subjected to a comprehensive ionization process utilizing the Agilent Dual electrospray ionization system, which can operate as an ESI source in both positive and negative modes, offering flexibility for sample analysis. The mass spectrometer, with its wide m/z range of 100–1000, facilitated the detection of various ions present in the samples, thereby enhancing the accuracy and precision of the analysis. The chromatographic separation was performed on a preheated C_{18} reversed-phase column (3.0 mm × 100 mm, Thermo Fisher Scientific, USA) at 35°C. The electrospray ionization conditions for MS were set as follows: ion source voltage, −4500 V; atomizing gas, 40 psi; auxiliary gas, 50 psi; air curtain gas, 25 psi; turbine gas temperature, 450°C; collision energy, 50 eV; and collision energy propagation, 40 eV. The complete process of acquiring data lasted for 10 minutes, guaranteeing swift and efficient analysis of the samples.

2.7. In Vitro Xanthine Oxidase Inhibition Assay. XOD inhibition activity was assessed using a modified protocol as previously described [15]. The weights of 0.7 g sodium dihydrogen phosphate, 2.1 g sodium hydrogen phosphate, and 0.9 g sodium chloride were measured and dissolved in 100 mL distilled water to prepare 0.1 mol/L phosphate buffer (PBS, pH 6.8). A working solution of XOD at a concentration of 0.1 U/mL was prepared by diluting the 10 U/mL XOD stock solution with PBS. To prepare a xanthine working solution with a concentration of 1 mmol/L, 1.5 mg xanthine powder was weighted and dissolved in 400 μL of 1 mol/L NaOH, followed by titration to a final volume of 100 mL using PBS. In brief, a 96-well plate was incubated with phosphate buffer (0.1 mL, pH 6.8), XOD (25 μL, 0.1 U/mL), and sample solution (25 μL). The mixture was subsequently subjected to incubation at 37°C for 20 min. Following this, 50 μL of xanthine (1 mmol/L) was added as substrate, and the reaction proceeded for five minutes at the same temperature. Absorbance values were measured at a wavelength of 290 nm using a microplate reader. For the blank control groups,

phosphate buffer was substituted for both the sample and xanthine reaction solutions, while in all the entire reaction groups, phosphate buffer replaced the sample solution. In addition, the sample control groups replaced the enzyme solution with phosphate buffer. Inhibition of the XOD inhibitory activity was determined using the following formula:

$$\text{Inhibition ratio}(\%) = \left(1 - \frac{C_3 - C_4}{C_2 - C_1}\right) \times 100\%. \quad (1)$$

C_3 represents the values of buffer, sample, substrate, and enzyme solution; C_4 represents the values of buffer, sample, and enzyme solution; C_2 represents the values of buffer, substrate, and enzyme solution; and C_1 represents the values of buffer and enzyme solution.

2.8. α-Amylase Inhibition Assay. The inhibition activity of αA was assessed using a modified protocol as previously described [16]. The weights of 0.14 g sodium dihydrogen phosphate, 0.42 g sodium hydrogen phosphate, and 0.18 g sodium chloride were measured and dissolved in 20 mL distilled water to prepare 20 mmol/L phosphate buffer (PBS, pH 6.8). A working solution of αA at a concentration of 4 U/mL was prepared by diluting the 50 U/mL αA stock solution with PBS. In brief, 100 μL of enzyme solution (4 U/mL, pH = 6.8) was mixed with 100 μL of each sample solution in an EP tube and incubated at 25°C for 5 min. Subsequently, the mixture was supplemented with 200 μL of starch solution (0.5%, w/v) and further incubated at the same temperature for 3 min. Afterwards, pipette 200 μL of the reaction mixture into a 1.5 mL EP tube followed by adding 100 μL DNS solution and heating at 85°C for 15 min. After cooling down, thorough mixing was achieved by adding 900 μL ultrapure water and ensuring even distribution throughout the mixture. The resulting mixed solution was then added to a 96-well plate with equal volumes in each well without exceeding its maximum capacity. Finally, the absorbance of each well at $\lambda = 540$ nm wavelength was measured using a BioTek microplate reader. This study chose acarbose as a positive control, and PBS buffer was used instead of αA. The calculation of αA inhibition rate can be determined using following formula:

$$\text{Inhibition ratio}(\%) = \left(1 - \frac{C_2 - C_3}{C_1}\right) \times 100\%. \quad (2)$$

Specifically, C_3 represents the values of sample and DNS; C_2 represents the values of enzyme solution, starch solution, and DNS; and C_1 represents the values of DNS and starch.

2.9. Pancreatic Lipase Inhibition Assay. The assessment of the inhibitory activity against PL was conducted using a protocol that has been modified by previous descriptions [15]. The p-nitrophenyl palmitate (p-NPP) substrate solution was prepared by dissolving 3.1 mg of p-NPP in 10 mL of Tris-HCl buffer (50 mmol/L), followed by heating at 45°C for 5 minutes, resulting in a concentration of 0.8 mmol/L. In triplicate tests, a 96-well plate was incubated with 20 μL sample solutions, 40 μL Tris-HCl buffer (50 mmol/L), and 60 μL enzyme solution (500 mg of PL was dissolved in a predetermined volume of Tris-HCl buffer in volumetric flasks, followed by centrifugation at a speed of 5000 rpm for 15 min). The mixture was incubated at a temperature of 37°C for a duration of 10 min, after which 80 μL p-NPP (0.8 mmol/L) was added as substrate. The mixture underwent further incubation at the same temperature for 30 minutes. The absorbance measurement using wavelength set at $\lambda = 405$ nm allowed quantification of inhibition percentage based on changes observed within sample wells compared to control groups. Positive control involved the utilization orlistat at concentration level equaling one milligram per milliliter. The calculation of PL inhibition rate can be determined using following formula:

$$\text{Inhibition ratio}(\%) = \left(1 - \frac{C_2 - C_4}{C_1 - C_3}\right) \times 100\%. \quad (3)$$

Specifically, C_2 represents the values of Tris-HCl, samples, substrates, and enzyme solutions; C_4 represents the values of Tris-HCl, samples, and substrates; C_1 represents the values of Tris-HCl, substrates, and enzyme solutions; and C_3 represents the values of Tris-HCl and substrates.

2.10. Molecular Docking. XOD (PDB code: 5N1X), αA (PDB code: 5EMY), and PL (PDB code: 1LPB) mentioned in the original sentence are all important proteins that play crucial roles in various physiological processes. The proteins mentioned above were acquired from the Protein Data Bank. Ligand and receptor synthesis were performed using PyMol 2.3 software, while Autodock Tools v1.56 package was employed for generating docking input files. For the analysis of receptor-ligand interactions, Discovery Studio 2021 was utilized. These protein structures offer valuable insights into their molecular interactions and potential functional modifications, which can be harnessed in the development of therapeutic interventions targeting diseases associated with these proteins.

2.11. Statistical Analysis. The experiments were meticulously designed and executed in triplicate to ensure the reliability and accuracy of the results. To further enhance the credibility of the findings, we employed two of the most widely used statistical software programs, SPSS software (IBM, version v26.0) and Origin 2021, to process and interpret the data. One-way ANOVA was employed to ascertain the presence of statistically significant variances among mean values (95% confidence level).

3. Results and Discussion

3.1. Separation of Bioactive Compounds. The complex procedure for extracting and refining compounds from *A. roxburghii*, an organism of great importance in natural product research, was effectively carried out using a wide range of sophisticated techniques. These techniques include using 70% ethanol extraction, widely employed as an

efficient method for isolating compounds from plant materials. Then, the obtained 70% ethanol extract was subjected to ethyl acetate extraction to obtain the ethyl acetate fraction. This fraction was then isolated using C18 reversed-phase and Sephadex LH-20, a powerful gel filtration chromatography technique that further purified the extracts. Subsequently, TLC and HPLC were employed to further refine the extracts and isolate the target compounds. Seven compounds were identified upon analysis of the ethyl acetate crude extracts (Figure 2), and the HPLC analysis of these compounds is shown in additional file (Supplementary File (available here)). They were characterized by ^{1}H NMR and ^{13}C NMR spectroscopy, and compared to published data to confirm their precise structures.

Among the seven compounds, compounds **4** and **6** were obtained from *A. roxburghii* for the first time, highlighting their novelty. Additionally, the MS spectra of compounds **1**–**7** provided further confirmation of their structures, underscoring their accuracy and reliability.

Compound **1** ($C_{28}H_{32}O_{16}$, 95.06% purity) appeared as a pale-yellow powder without any defined crystalline structure and displayed the precursor ion at m/z 625.1763 ($[M+H]^+$) under positive ionization made. The analysis of the NMR spectra for both ^{13}C and ^{1}H isotopes of compound 1, as presented in Tables 1 and 2, respectively, exhibited remarkable consistency with the data previously published [17]. Therefore, we confirm that compound **1** is isorhamnetin-3-O-rutinoside (narcissin).

Compound **2** ($C_{30}H_{36}O_{16}$, 98.24% purity) was a yellow oil and displayed the precursor ion at m/z 675.1896 ($[M+Na]^+$) under positive ionization made. The analysis of the NMR spectra for both ^{13}C and ^{1}H isotopes of compound **2**, as presented in Tables 1 and 2, respectively, exhibited remarkable consistency with the data previously published [18]. Therefore, we confirm that compound **2** is 4′,5-dihydroxy-3,3′,7-trimethoxyflavone-4′-O-*α*-L-rhamnopyranosyl-(1⟶6)-*β*-D-glucopyranoside.

Compound **3** ($C_{15}H_{12}O_3$, 96.84% purity) was a white powder and displayed the precursor ion at m/z 263.0679 ($[M+Na]^+$) under positive ionization made. The analysis of the NMR spectra for both ^{13}C and ^{1}H isotopes of compound **3**, as presented in Tables 1 and 2, respectively, exhibited remarkable consistency with the data previously published [19]. Therefore, we confirm that compound **3** is 4-methoxy-2,5-dihydroxy-phenathrene.

Compound **4** ($C_{18}H_{16}O_7$, 99.14% purity) was a yellow powder and displayed the precursor ion at m/z 345.0969 ($[M+H]^+$) under positive ionization made. The analysis of the NMR spectra for both ^{13}C and ^{1}H isotopes of compound **4**, as presented in Tables 1 and 2, respectively, exhibited remarkable consistency with the data previously published [20]. Therefore, we confirm that compound **4** is 5,4′-dihydroxy-3,3′,7-trimethoxy-flavone.

Compound **5** ($C_{18}H_{16}O_7$, 99.54% purity) was a yellow powder and displayed the precursor ion at m/z 367.0788 ($[M+Na]^+$) under positive ionization made. The analysis of the NMR spectra for both ^{13}C and ^{1}H isotopes of compound **5**, as presented in Tables 1 and 2, respectively, exhibited remarkable consistency with the data previously published [21]. Therefore, we confirm that compound **5** is 3,5-dihydroxy-7,3′,4′-trimethoxyflavone.

Compound **6** ($C_{11}H_{18}O_3$, 94.85% purity) was a yellow oil and displayed the precursor ion at m/z 221.1148 ($[M+Na]^+$) under positive ionization made. As shown in Tables 1 and 2, the NMR spectra of ^{13}C and ^{1}H for compound **6** were analyzed, and the data closely matched the published data [22]. Therefore, we confirm that compound **6** is 5-hydroxy-3,4-dimethyl-5-pentylfuran-2(5H)-one.

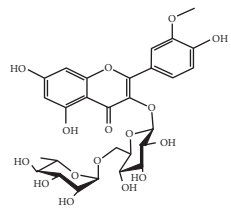
Compound **7** ($C_{16}H_{12}O_7$, 99.34% purity) was a yellow powder and displayed the precursor ion at m/z 317.0656 ($[M+H]^+$) under positive ionization made. The analysis of the NMR spectra for both ^{13}C and ^{1}H isotopes of compound **7**, as presented in Tables 1 and 2, respectively, exhibited remarkable consistency with the data previously published [23]. Therefore, we confirm that compound **7** is isorhamnetin.

3.2. Docking and Binding Free Energy. In order to evaluate the enzyme-inhibiting bioactive natural compounds derived from *A. roxburghii* against *α*A, XOD, and PL, comprehensive molecular docking studies were conducted. These studies aimed to examine the interaction between the compounds and the target enzymes to gain insights into their inhibitory action. The results of the lowest binding energies (BE, kcal/mol) of compounds **1**–**7** to these three enzymes are shown in Figure 3. It is widely acknowledged that a lower binding energy between the protein and substrate during docking increase complex stability [24]. The affinity of compound **1** and compound **5** for XOD was $-7.4\,\text{kcal mol}^{-1}$ and $-8.0\,\text{kcal mol}^{-1}$, respectively, as illustrated in Figure 3, indicating their significant binding capability to the enzyme and potent inhibition potential against XOD.

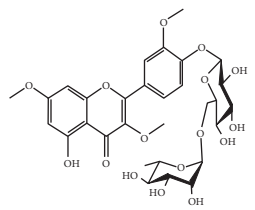
Moreover, compound **5** and compound **7** for *α*A were −8.0 kcal/mol and −8.0 kcal/mol, demonstrating a potent ability to inhibit its activity. The affinity of compound **1** (−9.1 kcal/mol) and compound **2** (−7.8 kcal/mol) for PL was more negative than −7.5 kcal/mol. These findings imply that the inhibitor exhibits a strong inclination to bind with these enzymes *in vitro*. The enhanced binding strength and notable interaction highlight the potential of these compounds as inhibitors, which can be further investigated and utilized to advance innovative therapeutic agents.

3.3. Measurement of Enzyme Inhibition Activity. Based on the molecular docking binding energies and the yield of the seven monomer compounds in *A. roxburghii*, we have assessed compounds **1**, **2**, **5**, **6,** and **7** for evaluating their activities against XOD, PL, and *α*A *in vitro* (Table 3).

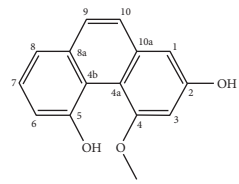
In Table 3, compound **5** (IC_{50}, $103.55 \pm 0.81\,\mu$g/mL), compound **6** (IC_{50}, $164.74 \pm 0.98\,\mu$g/mL), and compound **7** (IC_{50}, $289.74 \pm 4.54\,\mu$g/mL) exhibit inhibitory effects on XOD activity. However, it is crucial to highlight that the IC_{50}



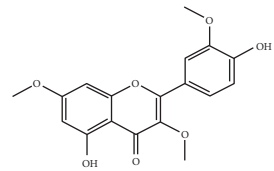
(1) Isorhamnetin-3-O-rutinoside



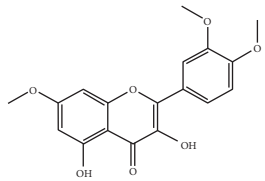
(2) 4',5-dihydroxy-3,3',7-trimethoxyflavone 4'-O-α-L-rhamnopyranosyl-(1→6)-β-D-glucopyranoside



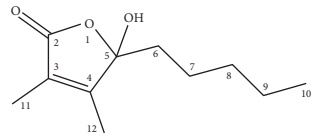
(3) 4-methoxy-2,5-dihydroxy-phenathrene



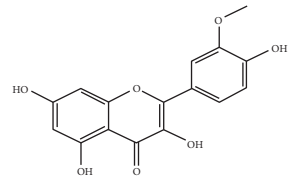
(4) 5,4'-dihydroxy-3,3',7-trimethoxy-flavone



(5) 3,5-dihydroxy-7,3',4'-trimethoxyflavone



(6) 5-hydroxy-3,4-dimethyl-5-pentylfuran-2 (5H)-one



(7) Isorhamnetin

Figure 2: Compounds obtained from *Anoectochilus roxburghii*.

Table 1: ^{13}C NMR data of compounds **1** – **7**[a].

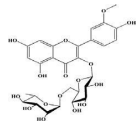
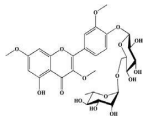
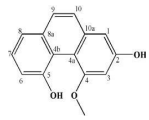
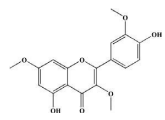
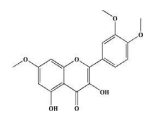
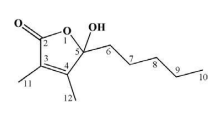
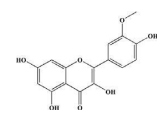
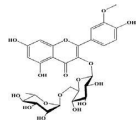
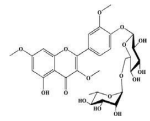
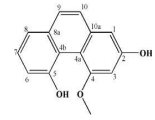
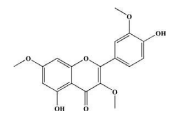
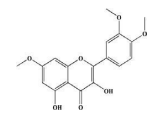
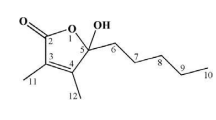
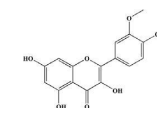
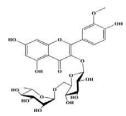
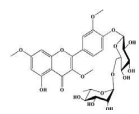
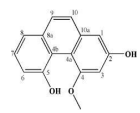
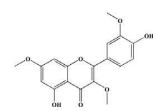
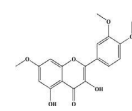
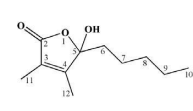
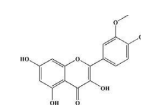
							
C1			106.1				
C2	158.5	157.3	155.4	147.5	146.6	174.7	147.3
C3	135.6	140.4	101.2	137.9	136.3	125.8	135.8
C4	179.4	180.2	156.5	178.0	176.1	160.5	175.9
C4a			111.9				
C4b			118.4				
C5	163.0	162.8	153.7	156.3	156.1	109.3	160.7
C6	100.1	99.2	115.5	97.8	97.5	37.1	98.2
C7	166.1	167.4	128.4	165.1	165.0	23.9	163.9
C8	95.1	93.5	119.9	92.4	92.1	32.9	93.6
C8a			133.4				
C9	158.9	158.3	126.3	160.9	160.3	23.7	156.1
C10	105.8	106.9	126.2	105.2	104.0	8.4	103.0
C10a			135.5				
C11						14.4	
C12						10.9	
C1′	123.1	123.4		122.3	123.2		121.9
C2′	114.7	113.7		115.6	111.5		111.7
C3′	148.4	150.6		149.9	148.4		148.8
C4′	150.9	150.4		155.8	150.5		146.6
C5′	116.2	117.2		112.0	110.9		115.5
C6′	124.1	125.9		120.7	121.6		121.7
Glc C1″[b]	104.6	102.3					
Glc C2″	76.0	74.9					
Glc C3″	78.3	78.0					
Glc C4″	71.7	71.6					
Glc C5″	77.4	77.2					
Glc C6″	68.7	67.9					
Rha C1‴[c]	102.6	102.1					
Rha C2‴	72.2	72.3					

Table 1: Continued.

							
Rha C3‴	72.4	72.5					
Rha C4‴	74.0	74.2					
Rha C5‴	69.9	70.0					
Rha C6‴	18.0	18.0					
C-3-OCH_3		60.9					
C-3′-OCH_3	55.9	57.0		56.1	55.7		55.8
C-7-OCH_3		56.7			56.1		
C-4-OCH_3			57.5	59.7			
C-4′-OCH_3				55.8	55.6		

[a]125 MHz measured in CD_3OD; [b]Glc for glucose; [c]Rha for rhamnose.

Table 2: ^{1}H NMR data of compounds 1–7[a].

							
H1			6.96 1H d				
H3			6.88 1H d				
H6	6.19 1H s	6.26 1H s	7.04 1H dd		6.36 1H d	1.94 2H m	6.20 1H s
H7			7.40 1H t			1.25 2H m	
H8	6.37 1H s	6.57 1H s	7.40 1H t	6.79 1H d	6.80 1H d	1.10 2H m	6.49 1H s
H9			7.62 1H d			1.72 2H m	
H10			7.52 1H d			0.89 3H t	
H11						1.93 3H d	
H12						1.78 3H d	
H1′							6.95 1H d
H2′	7.94 1H s	7.77 1H s		7.67 1H d	7.78 1H d		7.76 1H s
H5′	6.91 1H s	7.23 1H s		6.97 1H d	7.14 1H d		
H6′	7.61 1H s	7.77 1H s		7.63 1H dd	7.96 1H dd		7.69 1H d
Glc H1″[b]	5.24 1H s	5.00 1H s					
Glc H2″	3.65 1H s						
Glc H6″	3.84 1H d						
Glc H2″- H6	3.34 5H m	3.98 5H m					
Rha H1‴[c]	4.55 1H s	4.69 1H s					
Rha H2‴-H5‴	3.34 5H m	3.98 5H m					
Rha H6‴	1.12 3H d	1.18 3H d					
H-3-OCH_3		3.36 3H m		3.82 3H s			
H-4-OCH_3			4.06 3H s				
H-3′-OCH_3	3.95 3H s	3.61 3H m		3.87 3H s	3.85 3H d		3.85 3H s
H-4′-OCH_3				9.96 1H s	3.85 3H d		
H-7-OCH_3		3.62 3H m		3.87 3H s	3.88 3H s		
H-2-OH			10.05 1H s				
H-3-OH							9.77 1H s
H-5-OH			9.46 1H s	12.67 1H s	12.43 1H s		12.47 1H s
H-6-OH					9.67 1H s		
H-7-OH							10.83 1H s
H-4′-OH							9.44 1H s

[1]H NMR data of compounds 1-7[a]; [a]500 MHz measured in CD_3OD; [b]Glc for glucose; [c]Rha for rhamnose.

values of these three compounds under investigation are noticeably higher than those of the allopurinol (IC_{50}, $0.31 \pm 0.03\,\mu g/mL$). Notably, neither compound **1** nor compound **2** had significant effects on XOD, with almost negligible impact observed. Although compounds **5**, **6**, and **7** exhibit inhibitory effects on XOD activity, their potency is lower than the positive control drug. Further studies are needed to improve their potency and affinity towards the enzyme, which could lead to more potent and effective XOD inhibitors. Compounds **1**, **5**, and **7** have been found to

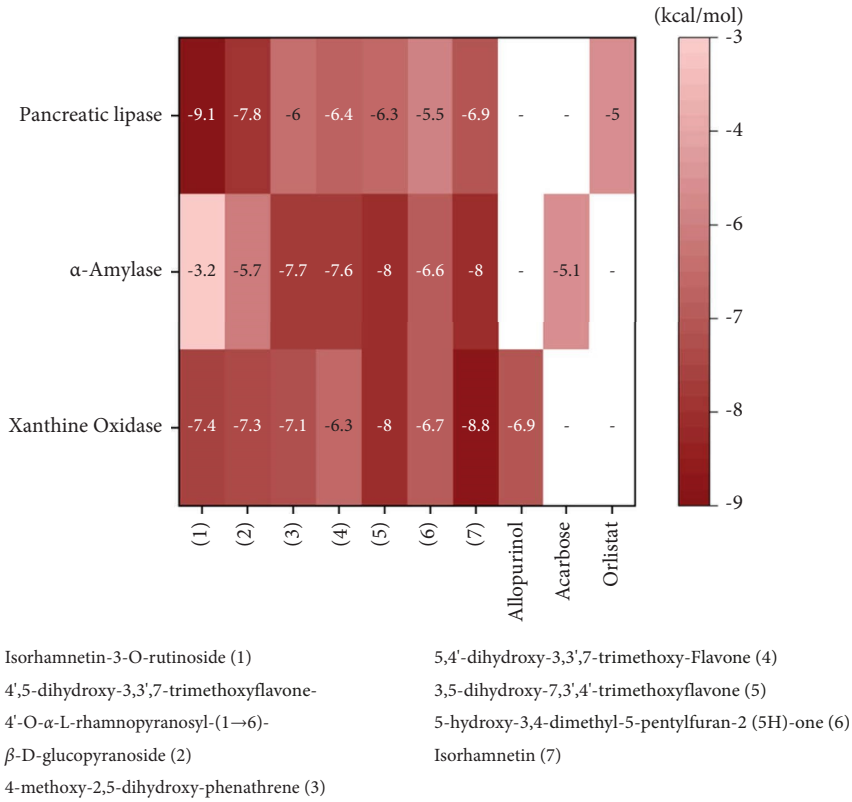


Figure 3: The lowest binding energies of compounds **1**–**7** with xanthine oxidase, α-amylase, and pancreatic lipase.

possess inhibitory properties against αA. Notably, compound **1** demonstrated a remarkable IC_{50} value of $87.45 \pm 1.77\,\mu g/mL$ and compound **7** showed an equally impressive IC_{50} of $190.29 \pm 3.34\,\mu g/mL$; these values indicate that both compounds are more potent inhibitors of αA than the positive control drug acarbose (IC_{50}, $233.76 \pm 1.71\,\mu g/mL$). The results demonstrated that compound **1** and compound **7** exhibited superior inhibitory effects on αA compared to acarbose, likely attributed to their distinct chemical structures. In addition to compounds **1** and **7**, some other compounds exhibited a comparatively lower degree of stimulation on αA activity, while others demonstrated no inhibitory effects. Postprandial hyperglycemia, a characteristic feature of diabetes, has the potential to cause complications in the retina, cardiovascular system, and kidneys. The activity of αA can be effectively inhibited to reduce blood glucose levels [25]. Compound **1**, compound **2**, compound **6**, and compound **7** showed weak inhibitory activity on PL. However, no PL inhibitory activity was observed for compound **5**. Utilizing the experimental findings from this study has the potential to facilitate the development of novel, cost-effective, and highly efficacious agents for hypoglycemia and uric acid reduction.

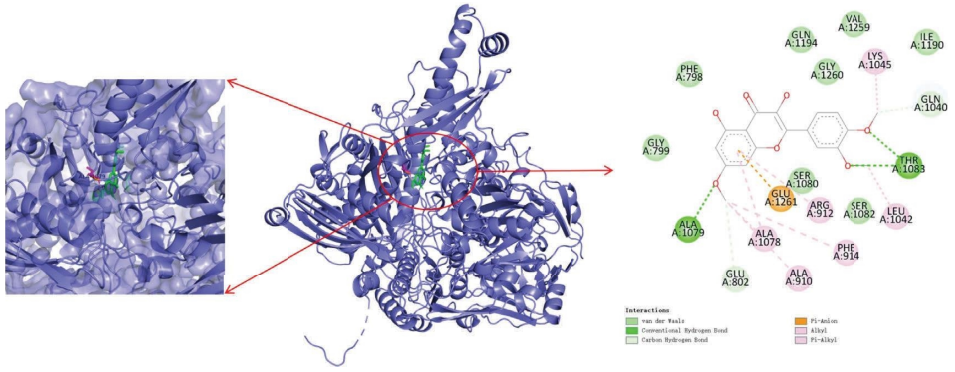
Moreover, the manufacturing process of these compounds requires implementing cost-effective strategies to enhance production efficiency and minimize waste. Furthermore, meticulous clinical trials involving a diverse range of participants are crucial to ensure the safety and efficacy of these drugs for widespread use. The findings of this study highlight the remarkable potential of *A. roxburghii* in lowering uric acid and blood glucose levels, paving the way for development of novel pharmaceuticals and functional foods.

3.4. Analysis of Molecular Docking Simulation Visualizations. Molecular docking is a powerful technique that enables the study of protein-ligand interactions at a molecular level, providing valuable information about the binding mode and affinity of the compounds. By simulating the binding process of the isolated compounds from *A. roxburghii* to XOD and αA, we could identify key residues that integrate a major binding site of these substrates and determine the critical interactions that lead to inhibition. The interactions between compounds **5** and **6** with XOD, as well as the interactions of compounds **1** and **5** with αA, are illustrated in Figure 4. The two enzymes establish a harmonious relationship with the compounds through intricate and diverse mechanisms, including hydrogen bond, π-π stacking, hydrophobic association, ligand coordination, and van der Waals forces. These various mechanisms work in unison to facilitate a stable and efficient interaction between the two enzymes and the compounds, enabling a wide range of chemical reactions to occur with precision and efficacy. These interactions demonstrate heightened affinity, suggesting the potential of compounds **5** and **6** in reducing uric acid levels. For molecular docking analysis with αA, compound **1** and compound **5** were selected. The three-dimensional

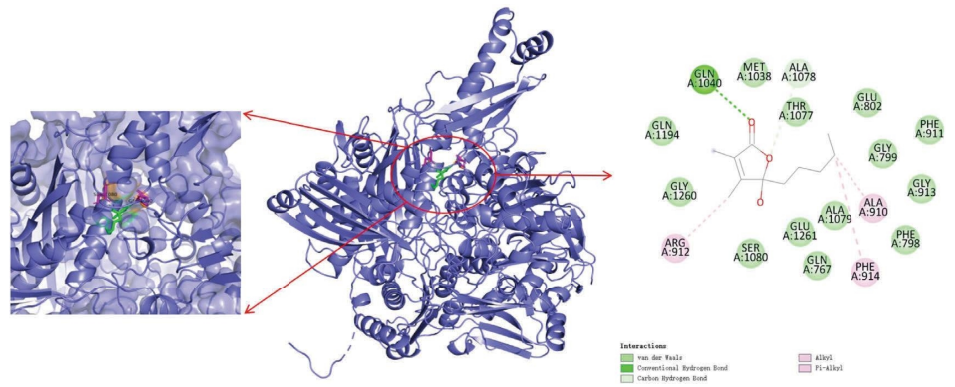
Table 3: Enzyme-inhibitory activity of compounds as determined with xanthine oxidase, α-amylase, and pancreatic lipase.

Compound	Xanthine oxidase IC_{50} (μg/mL)	α-Amylase IC_{50} (μg/mL)	Pancreatic lipase IC_{50} (μg/mL)
Isorhamnetin-3-O-rutinoside **(1)**	>500	87.45 ± 1.77^{a}	>500
4′,5-Dihydroxy-3,3′,7-trimethoxyflavone- 4′-O-α-L-rhamnopyranosyl-(1⟶6)-β-D-glucopyranoside **(2)**	>500	>500	>500
3,5-Dihydroxy-7,3′,4′-trimethoxyflavone **(5)**	103.55 ± 0.81^{b}	247.90 ± 1.71^{b}	ND
5-Hydroxy-3,4-dimethyl-5-pentylfuran-2(5H)-one **(6)**	164.74 ± 0.98^{c}	ND	>500
Isorhamnetin **(7)**	289.74 ± 4.54^{d}	190.29 ± 3.34^{c}	>500
Allopurinol	0.31 ± 0.03	—	—
Acarbose	—	233.76 ± 1.71	—
Orlistat	—	—	0.72 ± 0.02

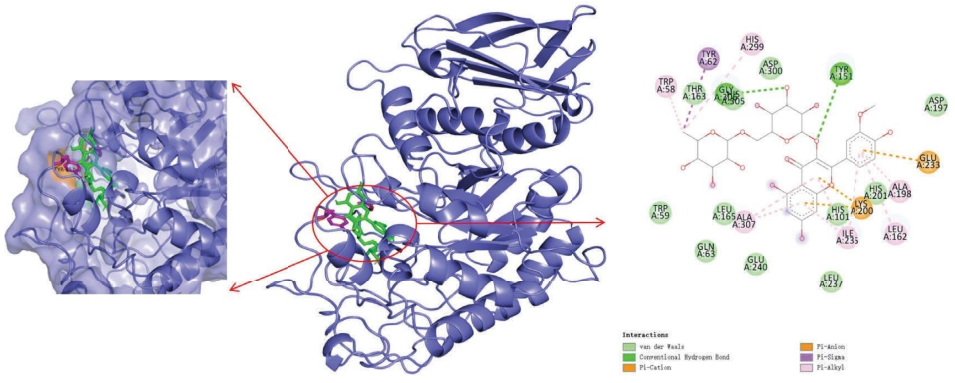
"ND" represents no activity was detected. Data are presented as mean values ± SD ($n = 3$). Different letters in the same column indicate a statistically significant difference ($p < 0.05$).



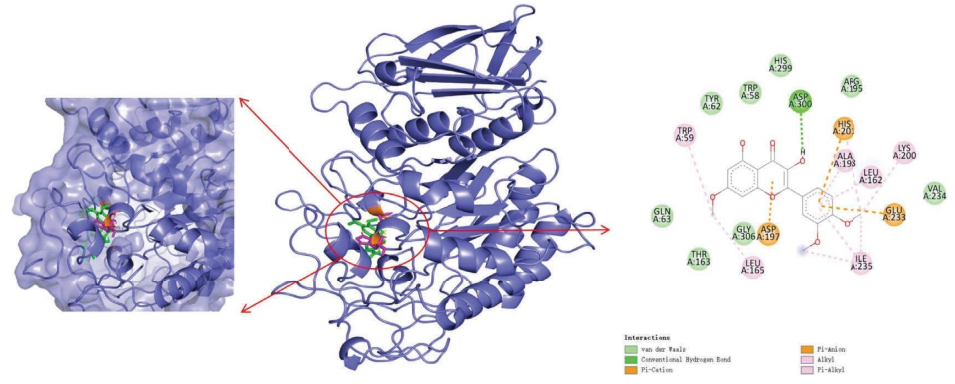
(a)



(b)



(c)



(d)

Figure 4: Molecular docking analysis of compound with protein. (a) and (b) Compound 5 and compound 6 (in green) into the binding site of xanthine oxidase (PDB ID. 1 N5X); (c) and (d) compound 1 and compound 5 (in green) into the binding site of α-amylase (PDB ID. 5EMY).

molecular docking diagram revealed the formation of hydrogen bonds between compounds **1** and **5** and their adjacent residues. Identification of additional residues, including HIS299, TRP59, LFU165, GLU233, and ILF235, near the ligand/αA complex has provided valuable insights into the intricate interactions between these molecules. Moreover, the highest-ranked substances exhibited hydrogen bonding, indicating their possibility to inhibit the enzymatic activity of XOD and αA, while suggesting a possible role in reducing uric acid levels and blood sugar. These findings highlight the promising applications of *A. roxburghii* extract in the pharmaceutical industry.

4. Conclusions

The Orchidaceae family member *Anoectochilus roxburghii* (Wall.) Lindl., a perennial plant, is used for medicinal and culinary purposes. It is widely used in human diets, pharmaceutical products, and pharmaceutical medicines. A combination of silica gel column chromatography, preparative thin-layer, RP-C18, Sephadex LH-20 column chromatography, and HPLC was employed to isolate seven active compounds from *A. roxburghii*, and subsequently their chemical structure composition was confirmed by nuclear magnetic resonance (^{1}H NMR, ^{13}C NMR). The compounds 5,4′-dihydroxy-3,3′,7-trimethoxy-flavone and 5-hydroxy-3,4-dimethyl-5-pentylfuran-2(5H)-one were obtained from *A. roxburghii* for the first time. The cumulative findings of our study demonstrate the therapeutic and protective effects of *A. roxburghii* in managing HUA and diabetes. With measurement of enzyme inhibition activity and molecular docking simulation analysis, 3,5-dihydroxy-7,3′,4′-trimethoxyflavone **(5)** demonstrates novel potential as a first-time inhibitor of XOD and αA for the first time. At the same time, 5-hydroxy-3,4-dimethyl-5-pentylfuran-2(5H)-one **(6)** exhibits promising inhibitory activity against XOD for the first time. Meanwhile, further in vivo and clinical studies are required to unravel the antidiabetic and anti-HUA activities. The results present promising perspectives for further investigations into these natural products' biological effects and medicinal applications.

Data Availability

Data are available upon reasonable request.

Conflicts of Interest

The authors declare that they have no conflicts of interest.

Authors' Contributions

Jiahao Yuan and Xiuna Wu were responsible for conceptualization, methodology, data curation, original draft preparation, and review and editing. Emad Karrar was responsible for formal analysis and visualization. Lingyu Zhang was responsible for project administration, data curation, and validation. Zhiyong Huang was responsible for data curation. Daren Wu was responsible for investigation. Jian Li was responsible for project administration, funding acquisition, and supervision. Jiahao Yuan and Xiuna Wu contributed equally to this work.

Acknowledgments

This work was supported by the National Natural Science Foundation of China (grant no. 32272322), the Key Science and Technology Project of Fujian Province (grant nos. 2021N5003 and 2022I0017), and the Natural Science Foundation of Fujian Province (grant no. 2021J01837).

Supplementary Materials

Supplementary file: the HPLC analysis of monomer compounds from *Anoectochilus roxburghii*. (*Supplementary Materials*)

References

[1] Y. Zhang, Y. Li, X. Chen, Z. Meng, and S. Guo, "Combined metabolome and transcriptome analyses reveal the effects of mycorrhizal fungus ceratobasidium sp. AR2 on the flavonoid accumulation in Anoectochilus roxburghii during different growth stages," *International Journal of Molecular Sciences*, vol. 21, no. 2, p. 564, 2020.

[2] Y. Qiu, W. Song, Y. Yang et al., "Isolation, structural and bioactivities of polysaccharides from Anoectochilus roxburghii (Wall.) Lindl.: a review," *International Journal of Biological Macromolecules*, vol. 236, 2023.

[3] S. C. Cui, J. Yu, X. H. Zhang, M. Z. Cheng, L. W. Yang, and J. Y. Xu, "Antihyperglycemic and antioxidant activity of water extract from Anoectochilus roxburghii in experimental diabetes," *Experimental and Toxicologic Pathology*, vol. 65, no. 5, pp. 485–488, 2013.

[4] H. B. Hsiao, J. B. Wu, H. Lin, and W. C. Lin, "Kinsenoside isolated from Anoectochilus formosanus suppresses LPS-stimulated inflammatory reactions in macrophages and endotoxin shock in mice," *Shock*, vol. 35, no. 2, pp. 184–190, 2011.

[5] Y. Guo, Q. Ye, S. Yang et al., "Therapeutic effects of polysaccharides from Anoectochilus roxburghii on type II collagen-induced arthritis in rats," *International Journal of Biological Macromolecules*, vol. 122, pp. 882–892, 2019.

[6] B. Zeng, M. Su, Q. Chen, Q. Chang, W. Wang, and H. Li, "Antioxidant and hepatoprotective activities of polysaccharides from Anoectochilus roxburghii," *Carbohydrate Polymers*, vol. 153, pp. 391–398, 2016.

[7] Y. Zhang, J. Cai, H. Ruan, H. Pi, and J. Wu, "Antihyperglycemic activity of kinsenoside, a high yielding constituent from Anoectochilus roxburghii in streptozotocin diabetic rats," *Journal of Ethnopharmacology*, vol. 114, no. 2, pp. 141–145, 2007.

[8] H. Gao, L. Ding, R. Liu et al., "Characterization of Anoectochilus roxburghii polysaccharide and its therapeutic effect on type 2 diabetic mice," *International Journal of Biological Macromolecules*, vol. 179, pp. 259–269, 2021.

[9] G. Buron-Moles, A. Chailyan, I. Dolejs, J. Forster, and M. H. Mikš, "Uncovering carbohydrate metabolism through a genotype-phenotype association study of 56 lactic acid bacteria genomes," *Applied Microbiology and Biotechnology*, vol. 103, no. 7, pp. 3135–3152, 2019.

[10] M. Kahaer, B. Zhang, W. Chen et al., "Triglyceride glucose index is more closely related to hyperuricemia than obesity indices in the medical checkup population in xinjiang, China," *Frontiers in Endocrinology*, vol. 13, 2022.
[11] S. Li, X. Lu, X. Chen et al., "The prevalence and associated clinical correlates of hyperuricemia in patients with bipolar disorder," *Frontiers in Neuroscience*, vol. 16, 2022.
[12] R. Wang, X. Yue, G. Shan et al., "A novel multi-hyphenated approach to screen and character the xanthine oxidase inhibitors from saffron floral bio-residues," *International Journal of Biological Macromolecules*, vol. 248, 2023.
[13] L. Zheng, G. Lin, R. Li et al., "Isochlorogenic acid C alleviates high-fat diet-induced hyperlipemia by promoting cholesterol reverse transport," *Frontiers in Pharmacology*, vol. 13, 2022.
[14] Q. Yue, Z. Wang, X. Tang et al., "Hypolipidemic effects of fermented seaweed extracts by *Saccharomyces cerevisiae* and lactiplantibacillus plantarum," *Frontiers in Microbiology*, vol. 12, 2021.
[15] J. Yuan, X. Wu, E. Karrar et al., "Identification of flavonoids in Anoectochilus roxburghii and in vitro inhibition of key enzymes relevant to metabolic syndrome," *Food Bioscience*, vol. 56, 2023.
[16] B. H. Abbasi, M. Shah, S. S. Hashmi et al., "Green bio-assisted synthesis, characterization and biological evaluation of biocompatible ZnO NPs synthesized from different tissues of milk thistle (Silybum marianum)," *Nanomaterials*, vol. 9, no. 8, p. 1171, 2019.
[17] G. Bader, D. Tuja, V. Wray, and K. Hiller, "Flavonol glycosides from heteropappus altaicus and H. Biennis," *Planta Medica*, vol. 59, no. 03, pp. 284-285, 1993.
[18] P. H. Nguyen, V. V. Dung, B. T. Zhao, Y. H. Kim, B. S. Min, and M. H. Woo, "Antithrombotic and antidiabetic flavonoid glycosides from the grains of Sorghum bicolor (L.) Moench var. hwanggeumchal," *Archives of Pharmacal Research*, vol. 37, no. 11, pp. 1394–1402, 2014.
[19] X.-M. Zhou, C.-J. Zheng, L.-S. Gan et al., "Bioactive phenanthrene and bibenzyl derivatives from the stems of dendrobium nobile," *Journal of Natural Products*, vol. 79, no. 7, pp. 1791–1797, 2016.
[20] H. Itokawa, K. Suto, K. J. C. Takeya, and P. Bulletin, "Studies on a novel p-coumaroyl glucoside of apigenin and on other flavonoids isolated from patchouli (Labiatae)," *Chemical and Pharmaceutical Bulletin*, vol. 29, no. 1, pp. 254–256, 1981.
[21] M. G. Phan, T. V. H. Do, and Q. B. Nguyen, "Methylated flavonols from amomum koenigii J.F.gmel. and their antimicrobial and antioxidant activities," *Biochemistry Research International*, vol. 2020, Article ID 4812312, 6 pages, 2020.
[22] J. Zhang, Y. Liang, X. J. Liao, Z. Deng, and S. H. Xu, "Isolation of a new butenolide from the South China Sea gorgonian coral Subergorgia suberosa," *Natural Product Research*, vol. 28, no. 3, pp. 150–155, 2014.
[23] Q. Zhang, W. Yang, J. Liu et al., "Identification of six flavonoids as novel cellular antioxidants and their structure-activity relationship," *Oxidative Medicine and Cellular Longevity*, vol. 2020, Article ID 4150897, 12 pages, 2020.
[24] S. Asgharzadeh, B. Shareghi, and S. J. I. J. o. B. M. Farhadian, "Structural alterations and inhibition of lysozyme activity upon binding interaction with rotenone: insights from spectroscopic investigations and molecular dynamics simulation," *International Journal of Biological Macromolecules*, vol. 254, 2024.
[25] A. Elbermawi, M. S. Darwish, A. A. El-Awady, A. A. Zaki, L. Qiu, and R. M. Samra, "Isolation and biological activities of compounds from Rumex vesicarius L. and their use as a component of a synbiotic preparation," *Food Chemistry X*, vol. 14, Article ID 100306, 2022.